Multiplexed Digital Holography for Atmospheric Characterization

Matthias T. Banet[1,*], Mark F. Spencer[2]

[1]*The Institute of Optics, University of Rochester, 480 Intercampus Drive, Rochester, New York 14627, USA*
[2]*Directed Energy Directorate, Air Force Research Laboratory, 3550 Aberdeen Avenue SE, Kirtland Air Force Base, New Mexico 87117, USA*

[*]*mbanet@ur.rochester.edu*

Abstract: Provided a coherently-illuminated object and a point-source beacon, multiplexed digital holography enables atmospheric characterization via complex-valued data. In this paper, we study two off-axis recording geometries which enable multiplexed digital holography and show that both perform well with respect to the field-estimated Strehl ratio.

OCIS codes: (010.1285) Atmospheric correction; (100.2000) Digital image processing;

1. Introduction

Digital holography, in practice, directly retrieves the wrapped phase of the complex-optical field. As such, we can resolve the branch points and associated branch cuts in the phase function [1]. These branch points and associated branch cuts result from total-destructive interference, whether from object-induced speckle, atmosphere-induced scintillation, or both. In addition, digital holography allows for a shot-noise limited detection regime given the interference between a weak signal beam and a strong reference beam [2–4].

With the benefits of digital holography in mind, there are several potential recording geometries that can be used. For example, the off-axis image-plane recording geometry (IPRG) [2], the off-axis pupil-plane recording geometry (PPRG) [3], and the on-axis phase-shifting recording geometry (PSRG) [4]. Previous work explored each of these recording geometries for the purposes of deep-turbulence wavefront sensing [2–4].

This paper studies the off-axis IPRG and PPRG and extends upon previous work by multiplexing two holograms in each camera exposure. Throughout, we assume that we have a coherently illuminated object and a point-source beacon (e.g., from a coherently illuminated ball-bearing object). In turn, we can perform both wavefront sensing and imaging (for the purposes of atmospheric characterization) using multiplexed digital holography, as shown in Fig. 1.

Fig. 1: Example Fourier planes (amplitude and wrapped phase) for the off-axis (a) IPRG and (b) PPRG. The red and blue boundaries represent the window functions that retrieve the complex-valued data from a coherently illuminated object and a point-source beacon, respectively.

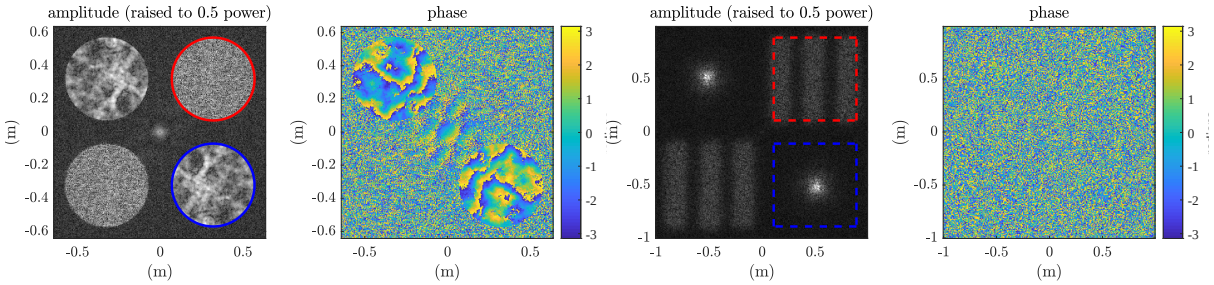

(a) IPRG Fourier plane

(b) PPRG Fourier plane

2. Simulation Setup

The work in this paper uses a wave-optics toolbox called WavePlex by Prime Plexus. That said, the simulations use the following propagation and detection geometries. Object light of wavelength $\lambda = 1\,\mu\text{m}$ propagates in the form of both a point-source beacon and a uniformly illuminated yet optically rough 3-bar object through 5 equally-spaced phase screens a total distance of $Z = 3.91\,\text{km}$ to an aperture of diameter $D = 0.5\,\text{m}$. At the aperture, we

collimate the object light to create a pupil plane and store the associated complex data in a 256 x 256 numerical grid. We vary the turbulence strength using the path-integrated Fried parameter r_0.

For the off-axis IPRG, we apply a thin lens to the pupil-plane fields and propagate to an image plane at focus which is where we place the focal-plane array (FPA). In contrast, for the off-axis PPRG, we place the FPA directly in the pupil plane. For both recording geometries, reference beams with distinct tilts interfere with their respective complex-optical fields and the FPA sums and stores the intensities from each interference pattern in units of photoelectrons (pe) (i.e., the holograms are mutually incoherent). The detection at the FPA includes shot noise, read noise, and a finite pixel-well depth [2, 3].

After detection, image processing techniques [a forward or inverse fast Fourier transform (FFT) followed by a windowing function] produce estimates of the complex-valued data in the pupil and image planes for both recording geometries. From these estimates, the simulations use several different metrics to gauge the performance of each recording geometry, including one in particular, the field-estimated Strehl ratio S_F. The reader should note that S_F gives a normalized gauge for performance and can be written as a function of the signal-to-noise ratio (SNR) [4], such that $S_F = \mathrm{SNR}/(1+\mathrm{SNR})$.

3. Results and Discussion

The results from the simulations show that both the off-axis IPRG and PPRG offer high-fidelity estimates of the complex-optical fields. As seen in Fig. 2, we computed the field-estimated Strehl ratio S_F for all of the turbulence strengths while varying SNRs [2, 3]. We observe in Fig. 2(a) that the value of S_F, which is for the object light recovered by the off-axis IPRG, remains just under the theoretical result for all turbulence strengths. In Fig. 2(b), S_F for the beacon return remains close to the theoretical result except for the weakest turbulence scenario. This deviation seems counter intuitive but ultimately results from pixel saturation.

Fig. 2: Field-estimated Strehl ratio results for the off-axis IPRG [cf. (a) and (b)] and PPRG [cf. (c) and (d)].

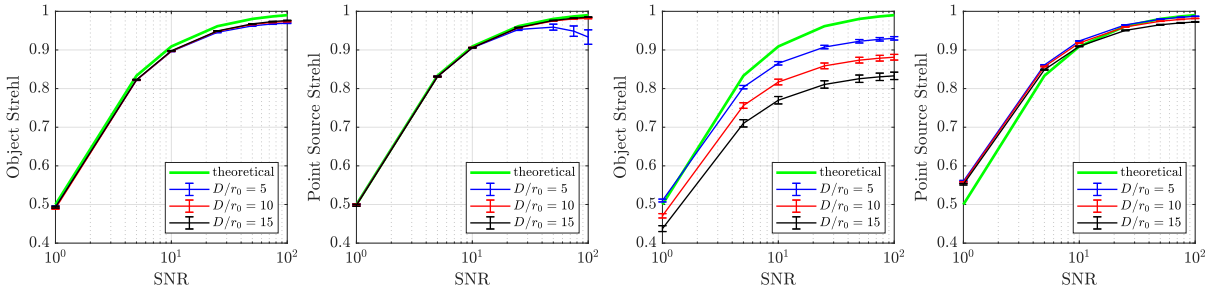

(a) Object S_F vs. SNR (IPRG)

(b) Point source S_F vs. SNR (IPRG)

(c) Object S_F vs. SNR (PPRG)

(d) Point source S_F vs. SNR (PPRG)

The results for the off-axis PPRG are shown in Fig. 2 as well. For the object return in Fig. 2(c), it is clear that stronger turbulence decreases the field-estimated Strehl ratio S_F overall compared to the theoretical result. Performance is worse than the off-axis IPRG because for this particular simulation the object takes up the entire width of the window function in the Fourier plane [cf. Fig. 1(b)], so that in stronger turbulence energy leaks outside the window function degrading the estimate. The results improve greatly for the simulations that use smaller objects. For the beacon return in Fig. 2(d), the results agree closely to the theoretical curve for all turbulence strengths, except it appears that S_F is higher than expected for low SNRs. The reason for this deviation is unknown at this time, but further exploration of the off-axis PPRG will hopefully elucidate this matter.

References

1. D. L. Fried, "Branch point problem in adaptive optics," J. Opt. Soc. Am. A **15**, 2759–2768 (1998).
2. M. F. Spencer et al., "Deep-turbulence wavefront sensing using digital-holographic detection in the off-axis image plane recording geometry," Optical Engineering **56**, 031213 (2016).
3. M. T. Banet et al., "Digital-holographic detection in the off-axis pupil plane recording geometry for deep-turbulence wavefront sensing," Appl. Opt. **57**, 465–475 (2018).
4. D. E. Thornton et al, "Deep-turbulence wavefront sensing using digital holography in the on-axis phase shifting recording geometry with comparisons to the self-referencing interferometer," Appl. Opt. **58**, A179–A189 (2019).